

Central Lancashire Online Knowledge (CLOK)

Title	The Origin of the Relation Between Stellar Angular Momentum and Stellar Mass in Nearby Disk-dominated Galaxies
Type	Article
URL	https://clok.uclan.ac.uk/id/eprint/43997/
DOI	https://doi.org/10.3847/2041-8213/ac911e
Date	2022
Citation	Du, Min, Ho, Luis C., Yu, Hao-Ran and Debattista, Victor P (2022) The Origin of the Relation Between Stellar Angular Momentum and Stellar Mass in Nearby Disk-dominated Galaxies. <i>The Astrophysical Journal Letters</i> , 937 (1). ISSN 2041-8213
Creators	Du, Min, Ho, Luis C., Yu, Hao-Ran and Debattista, Victor P

It is advisable to refer to the publisher's version if you intend to cite from the work.
<https://doi.org/10.3847/2041-8213/ac911e>

For information about Research at UCLan please go to <http://www.uclan.ac.uk/research/>

All outputs in CLoK are protected by Intellectual Property Rights law, including Copyright law. Copyright, IPR and Moral Rights for the works on this site are retained by the individual authors and/or other copyright owners. Terms and conditions for use of this material are defined in the <http://clok.uclan.ac.uk/policies/>



The Origin of the Relation Between Stellar Angular Momentum and Stellar Mass in Nearby Disk-dominated Galaxies

Min Du¹ , Luis C. Ho^{2,3} , Hao-Ran Yu¹ , and Victor P. Debattista⁴

¹ Department of Astronomy, Xiamen University, Xiamen, Fujian 361005, People's Republic of China; dumin@xmu.edu.cn

² Kavli Institute for Astronomy and Astrophysics, Peking University, Beijing 100871, People's Republic of China

³ Department of Astronomy, School of Physics, Peking University, Beijing 100871, People's Republic of China

⁴ Jeremiah Horrocks Institute, University of Central Lancashire, Preston, PR1 2HE, UK

Received 2022 June 16; revised 2022 August 17; accepted 2022 September 9; published 2022 September 23

Abstract

The IllustrisTNG simulations reproduce the observed scaling relation between the stellar specific angular momentum (sAM) j_s and mass M_s of central galaxies. We show that the local j_s - M_s relation $\log j_s = 0.55 \log M_s + 2.77$ develops at $z \lesssim 1$ in disk-dominated galaxies. We provide a simple model that describes well such a connection between halos and galaxies. The index of 0.55 of the j_s - M_s relation comes from the product of the indices of the $j_{\text{tot}} \propto M_{\text{tot}}^{0.81}$, $M_{\text{tot}} \propto M_s^{0.67}$, and $j_s \propto j_{\text{tot}}$ relations, where j_{tot} and M_{tot} are the overall sAM and mass of the halo, respectively. A non-negligible deviation from tidal torque theory, which predicts $j_{\text{tot}} \propto M_{\text{tot}}^{2/3}$, should be included. This model further suggests that the stellar-to-halo mass ratio of disk galaxies increases monotonically following a nearly power-law function that is consistent with the latest dynamical measurements. Biased collapse, in which galaxies form from the inner and lower sAM portion of their parent halos, has a minor effect at low redshifts. The retention factor of angular momentum reaches ~ 1 in disk galaxies with strong rotations, and it correlates inversely with the mass fraction of the spheroidal component, which partially explains the morphological dependence of the j_s - M_s relation.

Unified Astronomy Thesaurus concepts: Scaling relations (2031); Galaxy kinematics (602); Galaxy evolution (594); Spiral galaxies (1560); Galaxy dark matter halos (1880)

1. Introduction

The relation between the properties of galaxies and their parent dark matter halos, as well as the physical processes that regulate such properties, is a long-standing puzzle. In a cosmological framework, the angular momentum of a dark matter halo is initially acquired through tidal torques from neighboring perturbations. The classical tidal torque theory (Hoyle 1949; Peebles 1969) predicts that the specific angular momentum j_h (sAM hereafter) of halos follows $j_h \propto M_h^{2/3}$ where M_h is the halo mass (e.g., Peebles 1969; White 1984). If angular momentum is conserved throughout the formation of galaxies by accreting gas that decoupled from their host dark matter halos, a similar relation should also apply to galaxies. Observations show that the stellar masses M_s and sAM j_s of disk galaxies are correlated as a power law with an index of 0.52–0.64 (e.g., Fall 1983; Romanowsky & Fall 2012; Fall & Romanowsky 2013; Posti et al. 2018a; Di Teodoro et al. 2021; Mancera Piña et al. 2021a; Hardwick et al. 2022). This empirical trend is often called the “Fall relation”. The model $j_s \propto f_j f_m^{-2/3} M_s^{2/3} \lambda$ (Romanowsky & Fall 2012) has been widely used to explain the j_s - M_s relation. It requires that the retention factor of angular momentum $f_j \equiv j_s/j_h$, the stellar-to-halo mass ratio $f_m \equiv M_s/M_h$, and the spin parameter λ are independent of stellar mass. Unless these conditions are met, their dependence on stellar mass must conspire to cancel out to generate a correlation of the form $j_s \propto M_s^{2/3}$.

One of the key ingredients of the galaxy–halo connection is f_m or the stellar-to-halo mass relation (SHMR; reviewed by Wechsler & Tinker 2018). Within the general framework of abundance matching, the stellar-to-halo mass ratio peaks in halos around $10^{12} M_\odot$, assuming there is a little or no dependence on galaxy morphology. This result directly leads to a nonlinear j_s - M_s relation in logarithmic space, which is inconsistent with observations, as discussed by Posti et al. (2018b). Yet, several works suggest that the exact shape of the SHMR is not independent of galaxy morphology (e.g., Mandelbaum et al. 2006; Dutton et al. 2010; Rodriguez-Gomez et al. 2015; Posti & Fall 2021). Recently, Posti et al. (2019a, 2019b), using a sample of isolated disk galaxies with presumably more accurate halo masses measured dynamically, found that the SHMR follows a nearly linear relation in logarithmic space (see Di Teodoro et al. 2021, 2022 for some extremely massive cases). Zhang et al. (2022) reached a similar result for more than 20,000 star-forming galaxies whose dynamical masses were measured via galaxy–galaxy lensing and satellite kinematics.

Another key ingredient is the retention factor of angular momentum f_j . Disk-like structures grow at $z \lesssim 2$ by accreting cold gas from the vast reservoir of their circumgalactic medium (e.g., Tacchella et al. 2019; DeFelippis et al. 2020; Renzini 2020; Du et al. 2021). During this phase, the angular momentum of the gas should be conserved (up to a certain factor) to form disk galaxies with angular momenta tightly correlated with that of their parent dark matter halos. But no agreement is fully reached in studies that examined the link of the angular momentum amplitude between halos and galaxies. Zavala et al. (2016) and Lagos et al. (2017) found a remarkable connection between the sAM evolution of the dark and baryonic components of galaxies in EAGLE simulations. A



Original content from this work may be used under the terms of the [Creative Commons Attribution 4.0 licence](#). Any further distribution of this work must maintain attribution to the author(s) and the title of the work, journal citation and DOI.

similar correlation is suggested by Teklu et al. (2015) using the Magneticum Pathfinder simulation. Grand et al. (2017) and Rodriguez-Gomez et al. (2022) showed that the disk sizes and scale lengths are closely related to the angular momentum of halos in the Auriga and IllustrisTNG-100 simulations. However, Jiang et al. (2019) found little to no correlation using the NIHAO zoom-in simulation. A similar conclusion was drawn by Scannapieco et al. (2009) using eight Milky Way analogs. Danovich et al. (2015) argued that cold gas inflows cannot conserve angular momentum when they move into the inner regions of halos.

In this paper, we use IllustrisTNG (Pillepich et al. 2018a; Marinacci et al. 2018; Naiman et al. 2018; Nelson et al. 2018; Springel et al. 2018; Nelson et al. 2019; Pillepich et al. 2019) to revisit the long-standing open question of how the j - M relation develops in disk galaxies. We aim to address (1) whether or not there is a connection between the angular momentum of dark halos and that of the galaxies they host, (2) how the j_s - M_s evolves in disk galaxies, and (3) how the j_s - M_s relation can be explained using a simple theoretical model.

2. TNG50 Simulation and Data Reduction

IllustrisTNG is a suite of cosmological simulations that was run with gravo-magnetohydrodynamics and incorporates a comprehensive galaxy model (Weinberger et al. 2017; Pillepich et al. 2018b). The TNG50-1 run of the IllustrisTNG has the highest resolution. It includes 2×2160^3 initial resolution elements in a ~ 50 comoving Mpc box, corresponding to a baryon mass resolution of $8.5 \times 10^4 M_\odot$ with a gravitational softening length for stars of about 0.3 kpc at $z=0$. Dark matter is resolved with particles of mass $4.5 \times 10^5 M_\odot$. Meanwhile, the minimum gas softening length reaches 74 comoving pc. This resolution is able to reproduce the kinematic properties of galaxies with stellar mass $\gtrsim 10^9 M_\odot$ (Pillepich et al. 2019). The galaxies are identified and characterized with the friends-of-friends (Davis et al. 1985) and SUBFIND (Springel et al. 2001) algorithms. Resolution elements (gas, stars, dark matter, and black holes) belonging to an individual galaxy are gravitationally bound to its host subhalo.

In this work, we mainly focus on how the j_s - M_s relation develops in central galaxies dominated by disks. In such cases, neither mergers nor environmental effects have played an important role. We use the galaxies over the stellar mass range 10^9 – $10^{11.5} M_\odot$ from the TNG50-1 run. Disk-dominated galaxies are identified by $\kappa_{\text{rot}} \geq 0.5$, where $\kappa_{\text{rot}} = K_{\text{rot}}/K$ (Sales et al. 2012) denotes the relative importance of the cylindrical rotational energy K_{rot} over the total kinetic energy K measured for a given snapshot. Du et al. (2021) showed that $\kappa_{\text{rot}} \geq 0.5$ selects galaxies whose mass fractions of kinematically derived spheroidal structures are $\lesssim 0.5$. The other galaxies are classified as spheroid-dominated galaxies, which correspond to elliptical galaxies or slow rotators in observations. We further divide disk-dominated galaxies into two subgroups with $\kappa_{\text{rot}} \geq 0.7$ and $0.5 \leq \kappa_{\text{rot}} < 0.7$, which correspond to cases with strong rotation and with relatively moderate rotation, respectively, for a given snapshot. The former ones are likely to have a more disk-like morphology.

All the quantities in this paper are calculated using all particles belonging to galaxies/subhalos that include all gravitationally bound particles identified with the SUBFIND algorithm (Springel et al. 2001). We use only central galaxies that are primary subhalos of their parent halos. The sAM vector

is thus $\mathbf{j} = \sum_i \mathbf{J}_i / \sum_i m_i$, where \mathbf{J}_i and m_i are the angular momentum and mass of particle i , respectively. Galaxies are centered at the position with the minimum gravitational potential energy. No limitation on the radial extent is made to obtain the overall properties. The radial variation is ignored to simplify our discussion.

3. The Generation of the j_s - M_s Relation of Disk Galaxies at $z=0$

In the left-most panel of Figure 1, we show the j_s - M_s relation of galaxies at $z=0$ from TNG50, in comparison with those measured in observations. The shaded region encloses the fitting results of disk galaxies measured in the local universe (Romanowsky & Fall 2012; Fall & Romanowsky 2013; Posti et al. 2018a; Mancera Piña et al. 2021a; Hardwick et al. 2022). These studies concluded that j_s - M_s follows a well-defined linear scaling relation in logarithmic space with a slope of 0.52–0.64 and an rms scatter of ~ 0.2 dex. It is clear that TNG50 reproduces well the j_s - M_s relation observed in disk-dominated central galaxies (small blue and cyan dots). A linear fit (blue line) of all disk-dominated galaxies of TNG50 gives

$$\log j_s = (0.55 \pm 0.01) \log M_s - (2.77 \pm 0.11), \quad (1)$$

with a scatter (0.3 dex) similar to that observed. In this study, we adopt the linear regression and the least-squares method in fitting. The median trend (large blue dots) matches the linear fitting well. We focus on the general trend and physical origin of the j_s - M_s relation.

Figure 1 further shows that the j_s - M_s relation in the local universe develops at $z \lesssim 1$, which coincides well with the epoch of the formation and growth of disk galaxies. Its slope becomes shallower at higher redshifts, thus deviating from the j_s - M_s relation at $z=0$ (shaded regions); for example, $\log j_s = 0.34 \log M_s - 0.90$ at $z=1.5$. In the third panel of Figure 1, we can see that the disk galaxies at $z=0.5$ – 1.5 measured by Swinbank et al. (2017) follow a consistent distribution with the TNG50 disk galaxies. It is worth mentioning again that here the galaxies for each redshift are kinematically classified by κ_{rot} . At high redshifts, the spheroid-dominated galaxies follow a similar j_s - M_s relation as the disk-dominated cases, but with a larger scatter. As fewer disk-dominated galaxies form at higher redshifts, this result suggests that the growth of disk-like structures at late times ($z < 1$) is the key to establishing the locally observed j_s - M_s relation in disk galaxies.

The decrease of j_s toward high redshifts is most likely due to the effect of biased collapse (e.g., van den Bosch 1998), which predicts that gas with less angular momentum collapses earlier. The formation of galaxies at high redshifts thus is largely dominated by the assembly of spheroidal components whose angular momentum correlates weakly with that of their parent halos. The effect of biased collapse is gradually weakened toward low redshifts due to the assembly of disks by the accretion of gas with high angular momentum. In this study, we focus mainly on the generation of the j_s - M_s relation in disk-dominated galaxies at low redshifts. The effect of biased collapse is examined later in the paper.

4. A Physical Model of the j_s - M_s Relation

The existence of the j_s - M_s relation suggests that, despite the complexity of galaxy formation in a cosmological context, a

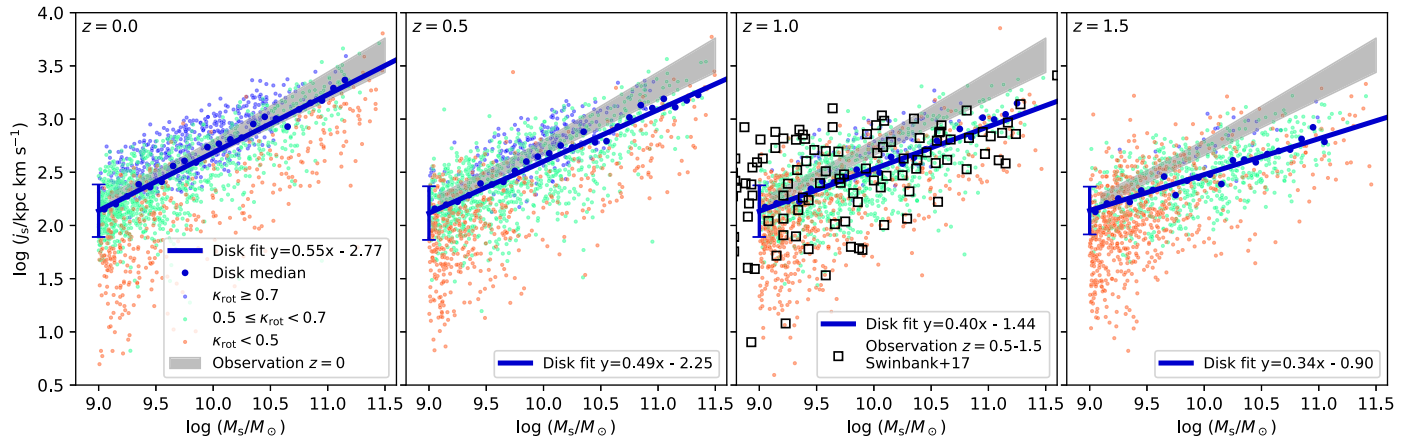


Figure 1. The evolution of the j_s - M_s relation in TNG50 from $z = 1.5$ to $z = 0$. The red, green, and blue symbols are central galaxies that correspond to spheroid-dominated galaxies with $\kappa_{\text{rot}} < 0.5$, disk-dominated galaxies with $0.5 \leq \kappa_{\text{rot}} < 0.7$, and disk-dominated galaxies with $\kappa_{\text{rot}} \geq 0.7$, respectively. The redshift is given at the top-left corner of each panel. The blue lines with error bars are the linear fitting results of disk-dominated galaxies. The error bars represent the standard deviation from the linear fitting, which is 0.3 dex at $z = 0$. The large blue dots show the trend of the median values. The shaded region shows the variance of the j_s - M_s relation suggested by observations at $z = 0$, where we combine the fitting results given by Romanowsky & Fall (2012), Fall & Romanowsky (2013), Posti et al. (2018a), Di Teodoro et al. (2021), and Mancera Piña et al. (2021a). In the third panel, the black squares show the j_s - M_s relation measured for disk galaxies at $z = 0.5$ –1.5 (Swinbank et al. 2017).

fundamental regularity still exists. This relation can be directly obtained by three simple equations

$$\log j_{\text{tot}} = \alpha \log M_{\text{tot}} + a, \quad (2)$$

$$\log M_{\text{tot}} = \beta \log M_s + f'_m, \quad (3)$$

$$\log j_s = \gamma \log j_{\text{tot}} + f'_j. \quad (4)$$

Here M_{tot} and j_{tot} are the total mass and angular momentum of a halo system, including baryonic and dark matter, respectively. This model yields

$$\log j_s = \alpha \beta \gamma \log M_s + a \gamma + \alpha \gamma f'_m + f'_j. \quad (5)$$

Equation (2) is a general form of the theoretical prediction of the halo j - M relation. Tidal torque theory suggests $\alpha = 2/3$, but if we allow for potential correction to the theory, α may deviate from $2/3$. As suggested by Posti et al. (2019a) (PFM19 hereafter), we assume that the stellar-to-halo mass ratio follows a single power-law relation (i.e., Equation (3) for disk galaxies). We apply Equation (4) to describe the retention of angular momentum, the retention factor is $f'_j = \log f_j$ if $\gamma = 1$.

In this section, we apply this simple model to the TNG50 data to show that they provide a good interpretation of the j_s - M_s relation. Section 4.1 shows the angular momentum correlation between halos and stars and then examines whether the effect of biased collapse is important. In Section 4.2, we show the SHMR and the j - M relation of halos, which play important roles in establishing the j_s - M_s relation. It is worth emphasizing that our results are based on a semi-quantitative analysis that is not sensitive to minor deviations from the scaling relations. All linear fitting results are roughly consistent with the trends of the median values over the mass range considered. We further discuss how our results challenge the SHMR obtained by the abundance matching method and the halo j - M relation predicted by tidal torque theory.

4.1. Angular Momentum Conservation during Disk Assembly

Previous works have suggested many phenomena that may induce angular momentum losses or gains, including dynamical

friction, hydrodynamical viscosity, galactic winds (e.g., Governato et al. 2007; Brook et al. 2011), and galactic fountains (e.g., Brook et al. 2012; DeFelippis et al. 2017). These processes, in conjunction with gas cooling and subsequent star formation, drive the circulation of gas in the circumgalactic medium.

The tight correlation between j_s and j_{tot} in central disk-dominated galaxies at $z = 0$ (Figure 2) verifies that the overall angular momentum is retained in a nearly constant ratio during star formation and gas circulation. This result supports the long-standing assumption from theory (e.g., Fall & Efstathiou 1980; Mo et al. 1998) and recent cosmological simulations (Teklu et al. 2015; Zavala et al. 2016; Lagos et al. 2017) that angular momentum is approximately conserved during galaxy formation. The galaxies with $\kappa_{\text{rot}} \geq 0.7$ match the $y = x$ line (thick dotted line), which suggests that angular momentum is conserved in galaxies with strong rotation, giving $j_s \sim j_{\text{tot}}$, namely $\gamma \sim 1$ and $f'_j \sim 0$. The disk-dominated galaxies with $0.5 \leq \kappa_{\text{rot}} < 0.7$ are slightly offset parallel to $y = x$. Equation (4) can thus be written as $\log j_s \simeq \log j_{\text{tot}} + f'_j$, where the offset f'_j decreases with κ_{rot} following a nearly parallel sequence. An accurate calculation of the median retention factors gives $f'_j = -0.07^{+0.15}_{-0.17}$ and $-0.21^{+0.20}_{-0.24}$ for disk-dominated galaxies with $\kappa_{\text{rot}} \geq 0.7$ and $\kappa_{\text{rot}} \geq 0.5$, respectively, which are consistent with the observational estimations for disk galaxies (Fall & Romanowsky 2013, 2018; Posti et al. 2019b; Di Teodoro et al. 2021). For comparison, the spheroid-dominated galaxies (median $f'_j = -0.63^{+0.31}_{-0.36}$) follow a weak correlation with a rather large scatter. They thus cannot be described by a linear relation.

It is worth emphasizing that the evolution of j_s is a cumulative effect that quantifies the overall conservation of angular momentum during past evolution. In Figure 3, we further show the relation between the sAM of the dark matter halo (j_h) and that of gas (j_g) and young stars. It is clear that j_g (upper panels) correlates linearly with j_h , but offsets toward higher sAM by about 0–0.5 dex, in qualitative agreement with the observations (Mancera Piña et al. 2021b). In the lower panels of Figure 3, we can see that the j_s for the young stars and

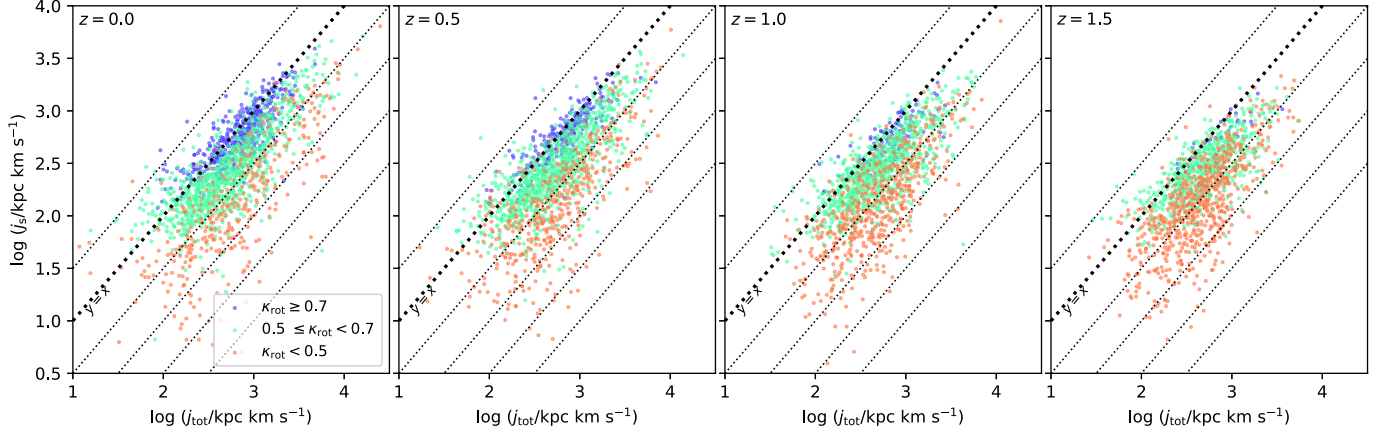


Figure 2. Evolution of the j_s - j_{tot} relation of central galaxies in TNG50. The red, green, and blue symbols are central galaxies that correspond to spheroid-dominated galaxies with $\kappa_{\text{rot}} < 0.5$, disk-dominated galaxies with $0.5 \leq \kappa_{\text{rot}} < 0.7$, and disk-dominated galaxies with $\kappa_{\text{rot}} \geq 0.7$, respectively. The dotted lines highlight the $\log j_s = \log j_{\text{tot}} + f'_j$ scaling relation in intervals of $\Delta f'_j = 0.5$.

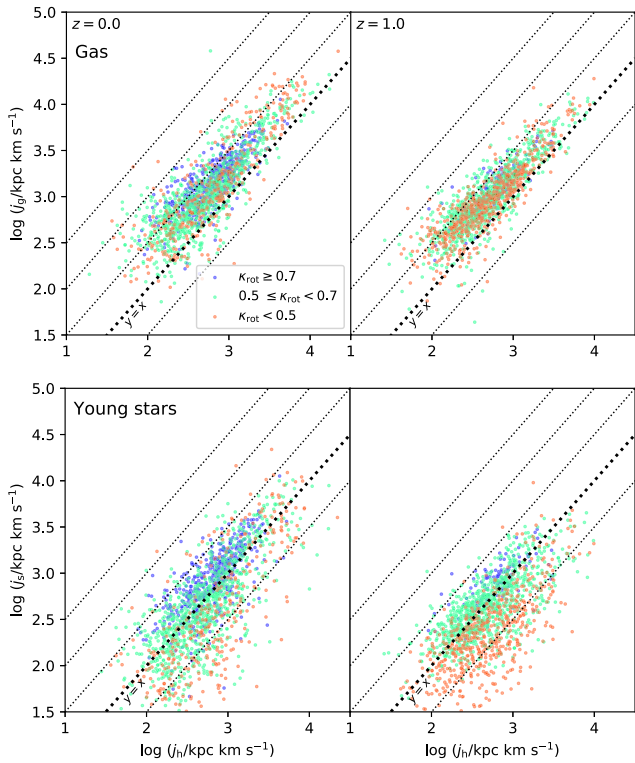


Figure 3. The evolution of the j - j_h relation for gas (top) and young stars (bottom) in TNG50 at $z = 0$ (left) and $z = 1.0$ (right). The red, green, and blue symbols are central galaxies that correspond to spheroid-dominated galaxies with $\kappa_{\text{rot}} < 0.5$, disk-dominated galaxies with $0.5 \leq \kappa_{\text{rot}} < 0.7$, and disk-dominated galaxies with $\kappa_{\text{rot}} \geq 0.7$, respectively. The dotted lines highlight the scaling relation in intervals of 0.5 dex. We exclude the cases with star formation rates lower than $0.1 M_\odot \text{ yr}^{-1}$ in the last 1 Gyr (i.e., quenched galaxies), which only contribute a small fraction ($\sim 1/4$ at $z = 0$) of even the spheroid-dominated galaxies.

j_h of disk-dominated galaxies (especially the cases with $\kappa_{\text{rot}} \geq 0.7$) follow roughly a similar linear scaling relation as the j_g - j_h relation at $z = 0$, albeit with a larger scatter and relatively lower sAM. Here the j_s of young stars is approximated using stars that form within 1 Gyr in each galaxy for a given snapshot. This result suggests that the sAM of gas and the

assembly of disks are largely determined by the sAM of their parent halos.

The fact that gas and young stars have higher sAM than dark matter can be partially explained by the biased collapse scenario (e.g., van den Bosch 1998). In this scenario, gas with lower angular momentum collapses earlier, whereupon the remaining gas, and consequently the young stars that form from it at lower redshifts, would be left with somewhat higher angular momentum. The conservation of sAM evidenced by Figure 2 suggests, however, that the overall effect of biased collapse has been quite modest in disk-dominated galaxies after a sufficiently long period of gas accumulation. A dramatic loss of angular momentum only occurs in spheroid-dominated galaxies, probably due to dry major mergers that can destroy the global rotation of their initial disks.

We further verify that the angular momentum vectors of the dark matter halo and stars are roughly aligned. Defining the misalignment angle θ as the angle between vectors j_s and j_h , the lower panel of Figure 4 shows that $\sim 60\%$ of disk-dominated galaxies have $\theta < 30^\circ$ at $z = 0$. This may induce a scatter on j_h by a factor of $< 1 - \cos 30^\circ = 0.13$, which is negligible. This result is consistent with previous studies (e.g., Bailin et al. 2005; Bett et al. 2010; Teklu et al. 2015; Shao et al. 2016). Motloch et al. (2021) further find a correlation between galaxy spin direction and halo spin reconstructed from cosmic initial conditions (Yu et al. 2020; Wu et al. 2021). We thus ignore the effect of orientation misalignment in this study, which uses disk-dominated galaxies.

We conclude that angular momentum is roughly conserved by a median factor of $f'_j \approx -0.21$ (corresponding to $j_s/j_{\text{tot}} \approx 0.62$) for disk-dominated central galaxies. A similar result is obtained in an independent analysis using the TNG100 run of IllustrisTNG (Rodriguez-Gomez et al. 2022). The overall correlation between galaxies and halos is maintained during the formation of disk-dominated galaxies. It is clear that the accretion of gas with high angular momentum dominates the growth of disk galaxies since $z = 1.5$. Without experiencing violent mergers, the assembly of disk-like structures is able to conserve angular momentum as stars form from the cold gas. While biased collapse has been considered to play an important role in interpreting the observed j_s - M_s relation (Shi et al. 2017;

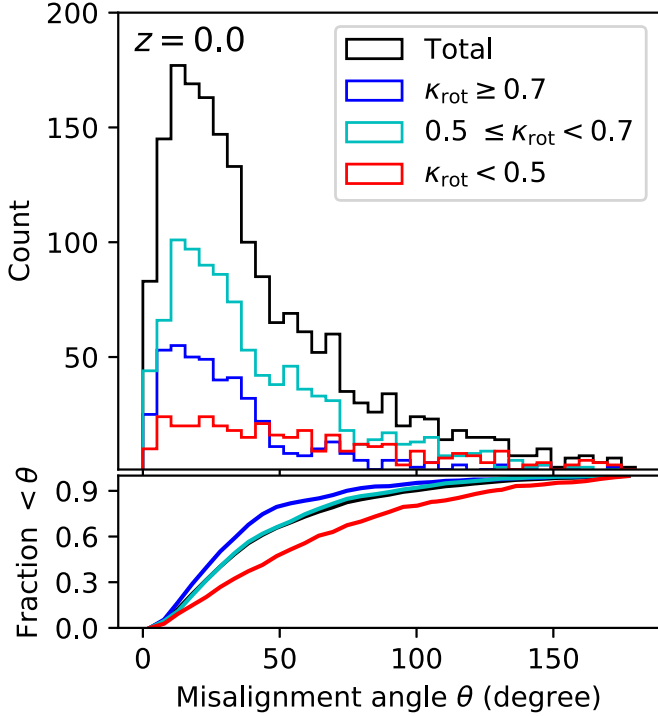


Figure 4. The number distribution of the misalignment angle θ (top) and its accumulative fraction (bottom) at $z = 0$. The misalignment angle θ measures the angle between vectors j_s and j_h . The three groups of galaxies are shown in blue, cyan, and red. The black curve corresponds to the distribution of all central galaxies.

Posti et al. 2018b), our results indicate that its effect has been largely erased in the local universe.

4.2. Constraining the j - M Relation of Halos with the SHMR

According to the j_s - j_{tot} relation, $\gamma \sim 1$, and therefore Equation (5) can be written as

$$\log j_s \simeq \alpha\beta \log M_s + a + \alpha f'_m + f'_j, \quad (6)$$

whose slope is determined by α and β . Tidal torque theory predicts $\alpha = 2/3$, which has been widely assumed. For this to hold, the index β of the SHMR must be close to 1.

In the upper panels of Figure 5, we show the M_s - M_{tot} relation of TNG50 galaxies. The linear fitting (dashed-dotted line) of disk-dominated galaxies (small blue and cyan dots) gives

$$\log M_{\text{tot}} = (0.67 \pm 0.01) \log M_s - (4.80 \pm 0.06), \quad (7)$$

at $z = 0$, according to which $\beta = 0.67$, significantly smaller than 1. We overlay the SHMR measured by PFM19 (black squares), who estimated halo masses directly from the kinematics of extended HI in central disk galaxies. The SHMR of TNG50 galaxies matches well with the results of PFM19, while it is systematically offset from that derived from the abundance matching method (e.g., Moster et al. 2013; the solid black profile) for massive galaxies. The abundance matching method suggests that the stellar-to-halo mass ratio follows a broken power-law relation peaking at $M_{\text{tot}} \approx 10^{12} M_{\odot}$ (Wechsler & Tinker 2018), assuming there is no dependence on galaxy morphology. In relatively less-massive galaxies with halo mass $< 10^{12} M_{\odot}$, both the observations of PFM19 and

simulations are consistent with abundance matching. The absence of a significant down-bending break in the SHMR of massive disk galaxies, however, challenges the results of abundance matching. While the SHMR of TNG50 galaxies is roughly consistent with that of PFM19, we do see a relatively minor down-bending break for $M_{\text{tot}} > 10^{12} M_{\odot}$ in TNG50. We have confirmed that the TNG100 simulation run in an 8 times larger box also exhibits a similar minor down-bending break. A similar result was obtained by Marasco et al. (2020) using the TNG100 run. They suggested that the active galactic nucleus feedback used in the TNG simulations is too efficient at suppressing star formation in massive disk galaxies. Here we simply use a linear fitting to describe the SHMR because (1) massive disk galaxies with $M_s \geq 10^{11} M_{\odot}$ that are offset significantly are rare, and (2) the difference from the median values (large blue dots) is minor.

The IllustrisTNG simulations suggest that there is a non-negligible correction to the $j \propto M^{2/3}$ relation when baryonic processes are considered. The lower panels of Figure 5 show the j_{tot} - M_{tot} relation. Using $\log j_{\text{tot}} - \log M_{\text{tot}}^{2/3}$ as the y -axis to highlight the discrepancy from the traditional tidal torque theory, the bottom-left panel clearly shows that the dark matter-only runs in the IllustrisTNG simulations indeed generate $j \propto M^{2/3}$ (TNG100-dark, corresponding to the dotted line and shaded regions), consistent with the theoretical expectation. However, in the presence of baryons, the j - M relation gradually deviates from this relation below $z = 1$ (lower panels of Figure 5). At $z = 0$, fitting the central galaxies dominated by disks from TNG50 gives

$$\log j_{\text{tot}} = (0.81 \pm 0.02) \log M_{\text{tot}} - (6.37 \pm 0.21). \quad (8)$$

The power-law index reaches $\alpha = 0.81$ at $z = 0$. Combining with the SHMR of disk-dominated galaxies (Equation (7))

$$\log j_s \simeq 0.54 \log M_s + f'_j - 2.48, \quad (9)$$

which explains perfectly the j_s - M_s index of 0.55 of disk galaxies at $z = 0$ (Figure 1). Apparently, the decrease of f'_j leads to a parallel shift of the j_s - M_s relation from disk-dominated toward more spheroid-dominated galaxies following a nearly parallel sequence. Shown in Figure 2 is $f'_j \approx 0$ for the galaxies with $\kappa_{\text{rot}} \geq 0.7$ at $z = 0$. For all disk-dominated galaxies ($\kappa_{\text{rot}} \geq 0.5$), for which $f'_j \approx -0.21$, Equation (9) gives $\log j_s \simeq 0.54 \log M_s - 2.69$, which predicts exactly the outcome of the j_s - M_s relation of disk-dominated galaxies at $z = 0$ (Equation (1)). The mass ratio of the spheroidal component quantified by κ_{rot} clearly correlates inversely with f'_j (Figure 2), offering a qualitative explanation for the morphological dependence of the j_s - M_s relation.

At high redshifts, the deviation from the local j_s - M_s relation is partially explained by the evolution of the j_{tot} - M_{tot} relation and the retention factor of angular momentum, as the M_{tot} - M_s relation remains nearly invariant since $z = 1.5$. The j_{tot} - M_{tot} and M_{tot} - M_s relations at $z = 1.5$ give $\log j_s = 0.46 \log M_s - 1.86$ in the case of $j_{\text{tot}} = j_s$, which still cannot fully explain the index of 0.34 of the j_s - M_s relation at high redshifts. This may be due to the fact that galaxies have been affected by biased collapse and by losses of angular momentum due to gas-rich mergers and clumpy instabilities at

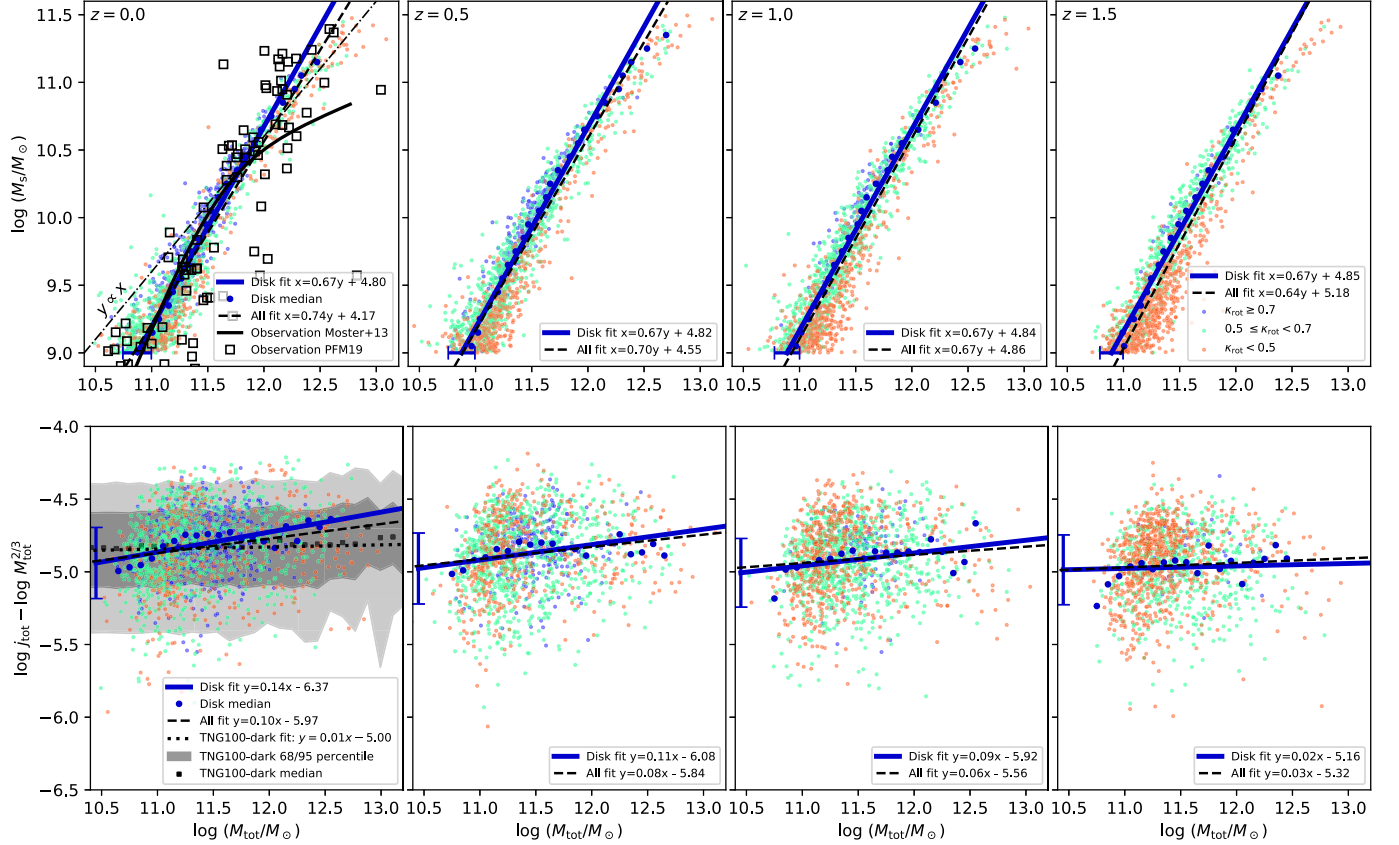


Figure 5. Evolution of the $M_{\text{tot}}-M_s$ and $j_{\text{tot}}-M_{\text{tot}}$ relations of central galaxies from $z = 1.5$ (right) to $z = 0$ (left) in TNG50. The red, green, and blue symbols are central galaxies that correspond to spheroid-dominated galaxies, disk-dominated galaxies with $0.5 \leq \kappa_{\text{rot}} < 0.7$, and disk-dominated galaxies with $\kappa_{\text{rot}} \geq 0.7$, respectively. In the upper panels, we overlay the observations of disk galaxies from PFM19 and Moster et al. (2013) for comparison. Both the linear fitting and medians are measured using equal bins in $\log M_s$, thus giving the parameters β and f'_m of Equation (3) directly. In the bottom panels, we normalize j_{tot} by $M_{\text{tot}}^{2/3}$ to highlight the discrepancy from tidal torque theory. In the bottom-left panel, the $j_{\text{tot}}-M_{\text{tot}}$ relation of central galaxies in TNG100-dark is overlaid for comparison. The shaded regions correspond to the 68 and 95 percentile envelopes. The dotted line and squares are the linear fitting result and median values, respectively.

$z > 1.5$, as a consequence of which the retention factor f'_j is smaller at high redshifts (right-most panel of Figure 2).

Our results suggest that the dark matter-only $j \propto M^{2/3}$ relation cannot explain the j_s-M_s relation. This is because the effect of central halos gaining angular momentum under the effect of baryonic processes needs to be included. The SHMR can be used to probe the $j-M$ relation in the local universe when the effect of biased collapse becomes insignificant. It is worth emphasizing that all conclusions above are mainly drawn using less-massive galaxies, whose SHMR can be described by a linear fit and is not sensitive to the down-bending break in massive ($M_{\text{tot}} > 10^{12} M_\odot$) galaxies.

The mechanism responsible for the discrepancy from the traditional tidal torque theory is still not well known. In previous studies, Zjupa & Springel (2017) suggested that the angular momentum in Illustris galaxies is underestimated by dark matter-only simulations for especially massive cases. Shown in their Figure 19, the spin parameter has indeed a weak dependence on halo mass ($M_h > 10^{11} M_\odot$) in a similar manner to our halo $j-M$ relation. We have verified that the disk-dominated galaxies in the TNG100 run have a similar discrepancy to the cases in TNG50 (see the result of TNG100 also in Figure 10 of Rodriguez-Gomez et al. 2022). Zhu et al. (2017) showed that the presence of the baryonic component can induce net rotation in the inner regions of dark matter halos, which may lead to an increase of their angular

momentum. Pedrosa et al. (2010) suggested that central galaxies may acquire angular momentum from their satellites that are disrupted by dynamical friction. Similarly, Lu et al. (2022) showed that galaxy interactions can inject angular momentum to the circumgalactic medium. Moreover, galaxies with relatively lower j_{tot} may have a higher probability of merger, thus transforming their morphology into ellipticals. We see that the slopes of all galaxies (black dashed lines) are slightly smaller, but they cannot fully explain the increase of j_{tot} .

5. Summary

In this paper, we show that the TNG50 simulation reproduces the observed scaling relation between the stellar SAM j_s and mass M_s of galaxies, as measured in the local universe. The disk-dominated central galaxies in TNG50 follow $\log j_s = 0.55 \log M_s - 2.77$, which matches the observations remarkably well. Our result confirms that the observed j_s-M_s relation may be regarded as evidence that the formation of disk galaxies is tightly correlated with dark matter halos. However, the theoretical $j-M$ relation ($j \propto M^{2/3}$) from dark matter-only simulations is not able to explain the j_s-M_s relation.

We show that the local j_s-M_s relation develops at $z \lesssim 1$ in disk galaxies. During this epoch, disk-like structures form or

grow significantly. Angular momentum is roughly conserved during the assembly of disk-like structures, which leads to a median retention factor of $\log j_s/j_{\text{tot}} = -0.07^{+0.15}_{-0.17} (-0.21^{+0.21}_{-0.24})$ for disk-dominated galaxies with $\kappa_{\text{rot}} \geq 0.7$ (0.5). The j_s - M_s relation of disk galaxies in the local universe can be well explained by a simple model with $j_{\text{tot}} \propto M_{\text{tot}}^{0.81}$, $M_{\text{tot}} \propto M_s^{0.67}$, and $j_s \propto j_{\text{tot}}$, where j_{tot} is the overall sAM and M_{tot} is the mass of the dark and baryonic components. Because of the cumulative accretion of mass with high angular momentum, the effect of biased collapse has been erased at low redshifts. The index of 0.55 of the j_s - M_s relation comes from the indices of the j_{tot} - M_{tot} and M_{tot} - M_s relations. We show that there is a non-negligible deviation from the halo $j \propto M^{2/3}$ relation, which explains the j_s - M_s relation. This model further suggests that the stellar-to-halo mass ratio of disk galaxies increases monotonically following a nearly power-law function, which is consistent with the latest dynamical measurement of disk galaxies. This challenges the general expectation from abundance matching that the stellar-to-halo mass ratio of disk galaxies decreases toward the massive end. Moreover, the retention factor of angular momentum inversely correlates with the mass ratio of spheroids, which possibly leads to the morphological dependence of the j_s - M_s relation.

We thank the anonymous referee for helpful suggestions. The authors acknowledge constructive comments and suggestions from S. M. Fall, L. Posti, S. Liao, and J. Shi. L.C.H. was supported by the National Science Foundation of China (11721303, 11991052, and 12011540375) and the China Manned Space Project (CMS-CSST-2021-A04 and CMS-CSST-2021-A06). M.D. and H.R.Y. acknowledge the support by the China Manned Space Program through its Space Application System, and the National Science Foundation of China 11903021 and 12173030. V.P.D. was supported by STFC Consolidated grant ST/R000786/1. The TNG50 simulation used in this work, one of the flagship runs of the IllustrisTNG project, has been run on the HazelHen Cray XC40-system at the High Performance Computing Center Stuttgart as part of project GCS-ILLU of the Gauss centers for Supercomputing (GCS). The authors are acknowledged for the help with the high-performance computing of Xiamen University. This work is also supported by the High-performance Computing Platform of Peking University, China.

ORCID iDs

- Min Du  <https://orcid.org/0000-0001-9953-0359>
 Luis C. Ho  <https://orcid.org/0000-0001-6947-5846>
 Hao-Ran Yu  <https://orcid.org/0000-0001-5277-4882>
 Victor P. Debattista  <https://orcid.org/0000-0001-7902-0116>

References

- Bailin, J., Kawata, D., Gibson, B. K., et al. 2005, *ApJL*, **627**, L17
 Bett, P., Eke, V., Frenk, C. S., Jenkins, A., & Okamoto, T. 2010, *MNRAS*, **404**, 1137
 Brook, C. B., Stinson, G., Gibson, B. K., et al. 2012, *MNRAS*, **419**, 771
 Brook, C. B., Governato, F., Roškar, R., et al. 2011, *MNRAS*, **415**, 1051
 Danovich, M., Dekel, A., Hahn, O., Ceverino, D., & Primack, J. 2015, *MNRAS*, **449**, 2087
 Davis, M., Efstathiou, G., Frenk, C. S., & White, S. D. M. 1985, *ApJ*, **292**, 371
 DeFelippis, D., Genel, S., Bryan, G. L., & Fall, S. M. 2017, *ApJ*, **841**, 16
 DeFelippis, D., Genel, S., Bryan, G. L., et al. 2020, *ApJ*, **895**, 17
 Di Teodoro, E. M., Posti, L., Ogle, P. M., Fall, S. M., & Jarrett, T. 2021, *MNRAS*, **507**, 5820
 Di Teodoro, E. M., Posti, L., Fall, S. M., et al. 2022, arXiv:2207.02906
 Du, M., Ho, L. C., Debattista, V. P., et al. 2021, *ApJ*, **919**, 135
 Dutton, A. A., Conroy, C., van den Bosch, F. C., Prada, F., & More, S. 2010, *MNRAS*, **407**, 2
 Fall, S. M. 1983, in Internal Kinematics and Dynamics of Galaxies, Proc. of the Symp., **100**, ed. E. Athanassoula (Dordrecht: Reidel), 391
 Fall, S. M., & Efstathiou, G. 1980, *MNRAS*, **193**, 189
 Fall, S. M., & Romanowsky, A. J. 2013, *ApJL*, **769**, L26
 Fall, S. M., & Romanowsky, A. J. 2018, *ApJ*, **868**, 133
 Governato, F., Willman, B., Mayer, L., et al. 2007, *MNRAS*, **374**, 1479
 Grand, R. J. J., Gómez, F. A., Marinacci, F., et al. 2017, *MNRAS*, **467**, 179
 Hardwick, J. A., Cortese, L., Obreschkow, D., Catinella, B., & Cook, R. H. W. 2022, *MNRAS*, **509**, 3751
 Hoyle, F. 1949, in Problems of Cosmical Aerodynamics, Proc. of a Symp., **195**, ed. H. C. Burgers & J. M. van de Hulst (Dayton, OH: Central Air Documents Office Army-Navy-Air Force)
 Jiang, F., Dekel, A., Kneller, O., et al. 2019, *MNRAS*, **488**, 4801
 Lagos, C. d. P., Theuns, T., Stevens, A. R. H., et al. 2017, *MNRAS*, **464**, 3850
 Lu, S., Xu, D., Wang, S., et al. 2022, *MNRAS*, **509**, 2707
 Mancera Piña, P. E., Posti, L., Frernali, F., Adams, E. A. K., & Oosterloo, T. 2021a, *A&A*, **647**, A76
 Mancera Piña, P. E., Posti, L., Pezzulli, G., et al. 2021b, *A&A*, **651**, L15
 Mandelbaum, R., Seljak, U., Kauffmann, G., Hirata, C. M., & Brinkmann, J. 2006, *MNRAS*, **368**, 715
 Marasco, A., Posti, L., Oman, K., et al. 2020, *A&A*, **640**, A70
 Marinacci, F., Vogelsberger, M., Pakmor, R., et al. 2018, *MNRAS*, **480**, 5113
 Mo, H. J., Mao, S., & White, S. D. M. 1998, *MNRAS*, **295**, 319
 Moster, B. P., Naab, T., & White, S. D. M. 2013, *MNRAS*, **428**, 3121
 Motloch, P., Yu, H.-R., Pen, U.-L., & Xie, Y. 2021, *NatAs*, **5**, 283
 Naiman, J. P., Pillepich, A., Springel, V., et al. 2018, *MNRAS*, **477**, 1206
 Nelson, D., Pillepich, A., Springel, V., et al. 2018, *MNRAS*, **475**, 624
 Nelson, D., Springel, V., Pillepich, A., et al. 2019, *ComAC*, **6**, 2
 Pedrosa, S., Tissera, P. B., & Scannapieco, C. 2010, *MNRAS*, **402**, 776
 Peebles, P. J. E. 1969, *ApJ*, **155**, 393
 Pillepich, A., Nelson, D., Hernquist, L., et al. 2018a, *MNRAS*, **475**, 648
 Pillepich, A., Springel, V., Nelson, D., et al. 2018b, *MNRAS*, **473**, 4077
 Pillepich, A., Nelson, D., Springel, V., et al. 2019, *MNRAS*, **490**, 3196
 Posti, L., & Fall, S. M. 2021, *A&A*, **649**, A119
 Posti, L., Frernali, F., Di Teodoro, E. M., & Pezzulli, G. 2018a, *A&A*, **612**, L6
 Posti, L., Frernali, F., & Marasco, A. 2019a, *A&A*, **626**, A56
 Posti, L., Marasco, A., Frernali, F., & Famaey, B. 2019b, *A&A*, **629**, A59
 Posti, L., Pezzulli, G., Frernali, F., & Di Teodoro, E. M. 2018b, *MNRAS*, **475**, 232
 Renzini, A. 2020, *MNRAS*, **495**, L42
 Rodriguez-Gomez, V., Genel, S., Vogelsberger, M., et al. 2015, *MNRAS*, **449**, 49
 Rodriguez-Gomez, V., Genel, S., Fall, S. M., et al. 2022, *MNRAS*, **512**, 5978
 Romanowsky, A. J., & Fall, S. M. 2012, *ApJS*, **203**, 17
 Sales, L. V., Navarro, J. F., Theuns, T., et al. 2012, *MNRAS*, **423**, 1544
 Scannapieco, C., White, S. D. M., Springel, V., & Tissera, P. B. 2009, *MNRAS*, **396**, 696
 Shao, S., Cautun, M., Frenk, C. S., et al. 2016, *MNRAS*, **460**, 3772
 Shi, J., Lapi, A., Mancuso, C., Wang, H., & Danese, L. 2017, *ApJ*, **843**, 105
 Springel, V., White, S. D. M., Tormen, G., & Kauffmann, G. 2001, *MNRAS*, **328**, 726
 Springel, V., Pakmor, R., Pillepich, A., et al. 2018, *MNRAS*, **475**, 676
 Swinbank, A. M., Harrison, C. M., Trayford, J., et al. 2017, *MNRAS*, **467**, 3140
 Tacchella, S., Diemer, B., Hernquist, L., et al. 2019, *MNRAS*, **487**, 5416
 Teklu, A. F., Remus, R.-S., Dolag, K., et al. 2015, *ApJ*, **812**, 29
 van den Bosch, F. C. 1998, *ApJ*, **507**, 601
 Wechsler, R. H., & Tinker, J. L. 2018, *ARA&A*, **56**, 435
 Weinberger, R., Springel, V., Hernquist, L., et al. 2017, *MNRAS*, **465**, 3291
 White, S. D. M. 1984, *ApJ*, **286**, 38
 Wu, Q., Yu, H.-R., Liao, S., & Du, M. 2021, *PhRvD*, **103**, 063522
 Yu, H.-R., Motloch, P., Pen, U.-L., et al. 2020, *PhRvL*, **124**, 101302
 Zavala, J., Frenk, C. S., Bower, R., et al. 2016, *MNRAS*, **460**, 4466
 Zhang, Z., Wang, H., Luo, W., et al. 2022, *A&A*, **663**, A85
 Zhu, Q., Hernquist, L., Marinacci, F., Springel, V., & Li, Y. 2017, *MNRAS*, **466**, 3876
 Zjupa, J., & Springel, V. 2017, *MNRAS*, **466**, 1625